

A novel structure proposal for distributed generation using SMES and PV system with relative controllers design

P. Naderi · F. Fallahi

Received: 26 September 2013 / Accepted: 2 September 2014 / Published online: 23 September 2014
© Springer-Verlag Berlin Heidelberg 2014

Abstract A combined power source including superconductor magnetic energy storage system (SMES) and photovoltaic (PV) systems has been considered for distributed generation system as a hybrid power source in this research. Both power sources have been connected to power grid and some controllers have been designed for power injection control. The SMES system can be in charging mode via PV system and power grid. Moreover, power injection controller has been designed for tuning of produced power of PV and SMES system. For this aim, a DC/DC converter has been connected to PV system and a bi-directional-three-level chopper has been used for SMES. PV power control has been based on the DC/DC converter control and the chopper control has been used for SMES power control. On the other hands, inverter control has been confirmed for injection of active/reactive power from distributed generation system to power grid. Proposal of a new scheme and design of a novel controller, are the advantages of this research. Finally, a series of simulation results have been shown.

Keywords PV system · SMES · Bi-directional-three-level chopper · Chopper switching · Three level inverter · Power injection

List of symbols

A The ideal coefficient related to photovoltaic cell model
 I_{SMES} The battery current

P. Naderi (✉) · F. Fallahi
Shahid Rajaei Teacher Training University, Tehran, Iran
e-mail: p.naderi@srttu.edu

F. Fallahi
e-mail: f.falahi@srttu.edu

I_{PH}	The current source related to photovoltaic system model
I_{SC}	The short circuit current of the diode used in the photovoltaic cell model
I_{RS}	The short reversed saturated current of the diode used in the photovoltaic cell model
K	Boltzmann constant
K_I	The temperature effect coefficient on the current of used diode in the photovoltaic cell model
N_s	The number of series cells in photovoltaic package
N_p	The number of parallel cells in photovoltaic package
P_{PV}	The power of photovoltaic system
P_{Tr}	The transmitted active power from the distributed generation system into the power grid
P_{PV-Max}	The maximum accessible power from the photovoltaic system
q	The numerical value of electron
Q_{Tr}	The transmitted reactive power from the distributed generation system into the power grid
R_s	The series resistor of each diode in photovoltaic package
R_{sh}	The parallel resistor of each diode in photovoltaic package
T_c	The temperature of the environment in photovoltaic system
T_{ref}	The reference temperature in photovoltaic system model
V_{c1}, V_{c2}	DC-link capacitors voltage
V_{DC}	The DC-link voltage which is equal to the addition of the capacitors voltage
f	The base frequency(the frequency of the inverter's modulation waves)
f_0	The resonance frequency of LCL filter
φ	The phase angle of the inverter's modulation waves
λ	The radiation coefficient in photovoltaic system model

1 Introduction

Distributed generation (DG) resources due to their inherent features like feeding local loads and continuous and economical operation have been given a lot of consideration from researchers in recent years. This is very good idea for power system growing in terms of economic, climate mitigation and also power system reliability [1, 2]. For this reason, different structures together with several control algorithms within research area have been proposed so far. Hence, energy storage units such as batteries, capacitors and coils are the essential elements for renewable energy systems [3]. There are some power sources which can be used as the energy resource such as photovoltaic (PV) and superconductor magnetic energy storage system (SMES) that are considered as combined source in this paper. However some papers addressed each one for distributed generation but a hybrid source including both has been not investigated yet in which considered in this work. The SMES is an inductor that can store large amount of electric energy in the form of magnetic flux by flowing DC current through its coil without experiencing losses. SMES systems have attracted the attention of both electric utilities and the military due to their fast response and high efficiency

(a charge/discharge efficiency over 95 %) [4]. The most important advantages of SMES devices include high power and energy density with outstanding conversion efficiency, unlimited number of charging and discharging cycles, much longer lifetime compared to the battery storage systems and fast and independent power response in four-quadrants [5,6]. As a new sample work, in [7] the SMES was used as a single source for distributed generation and a new controlling method was introduced but there was not addressed a hybrid source for DG. On the other hands, photovoltaic system is another energy resource which has been addressed in some researches. As a sample in [8] a PV source system is proposed in a wide area power system and measurement control has been addressed but a hybrid energy source has been not investigated. Maximum power point tracking (MPPT) is a more important factor in the PV systems. The MPPT is based on both irradiance and temperature [9]. Moreover, similarly to SMES, some converters should be used in PV system for its connecting to power grid. Regarding to investigate to energy storage components which can be used as DG power source, a good idea for energy resource is a hybrid source for using in a DG system. Naderi in [10] showed a hybrid distributed generation system using hybrid battery/photovoltaic system. The MPPT was performed and the control of active and reactive powers was investigated according to state of charge (SoC) of battery. Furthermore, in this method there is no reactive power control and bi-level inverter is used. In [11] a hybrid source including a combustion engine and a PV system was used for energy source of a DG system and a control strategy was introduced. In [12], a control strategy influence on the efficiency of a hybrid PV-Battery-Fuel Cell system was investigated for DG system and cost management was considered for control strategy and in [13] a nonlinear control strategy for PV-Fuel cell hybrid source was introduced in which MPPT has been addressed and converter using include of DC/DC and DC/AC was investigated. In [14], another hybrid source with CHP/PV system was investigate for in-house power backup and in [15], modeling and control of hybrid wind/PV/Fuel cell DG system was introduced and relative controllers were designed. Noticing to performed researches in DG area, in addition to storage components, the power electronic converters are other essential equipment which should be considered in DG systems. However DC/DC and DC/AC converters are used in many papers but DC chopper that is a special component is more important for SMES using. This paper presents a new control method for a three-level-bi-directional chopper in a hybrid DG system. In [16], an algorithm was presented base on a new switching method but a high frequency triangular wave was used for switching and high speed switches were considered. In [17] a 4-quadrant chopper was introduced for controlling of capacitors used in a five-level inverter but the SMES coil connecting to the mentioned chopper is not possible. In an old work [18], presents a new, optimized PWM scheme and control approaches for a three-level two-quadrant chopper in a SMES power conditioning system (PCS) but, many switch were used in chopper structure. In [19] a multi-level buck-boost controller was investigated with voltage controller method but it is a voltage feed converter and is not a good choice for SMES application. The hybrid power source for distributed generation needs to optimization algorithms [20,21] and also power source sizing [2] in which addressed in recent decade. Now in this paper a hybrid DG structure is considered by SMES-PV system and a current feed three-level-bi-directional chopper is introduced with a novel controlling method. The paper

is organized in eight sections. In the Sect. 2, considered structure for distributed generation issue using SMES and PV system is presented and the photovoltaic system model with maximum power point tracking is explained in Sect. 3 with presenting of a way for its power controlling through a DC/DC converter. In the Sect. 4, the way of controlling SMES through a chopper is presented and in the Sect. 5, the applied inverter is explained. Designed harmonic filter is illustrated in Sect. 6 and a fuzzy controller for controlling of active and reactive power followed into the power grid is designed in the Sect. 7. Finally, the proposed structure is verified through simulation results.

In general, the advantageous points of this paper in comparison with other available papers could be categorized as follows:

1. Using of SMES/Photovoltaic hybrid system as a distributed generation resource which is offered in this paper as a novel structure.
2. Presenting a novel structure for controlling bi-directional-three-level chopper connected to SMES which was offered by the researcher of this paper for the first time. The mentioned structure, in addition to its quick and accurate control system, provides the ability of direct connection of chopper to SMES.

2 Proposed structure

The proposed structure based on SMES and photovoltaic system which first proposed in this paper, is shown in Fig. 1. The maximum power of photovoltaic system varies according to temperature, so after estimating the power, a DC/DC converter regulates the received power on the maximum value. SMES system is connected to a bi-directional chopper and both DC-link voltage and connected capacitor bank are regulated through chopper switching. With regard to the connection of a three-level inverter to the group consisting of SMES and photovoltaic, it is required that the voltage of capacitors in capacitor bank is controlled equally. The control of the

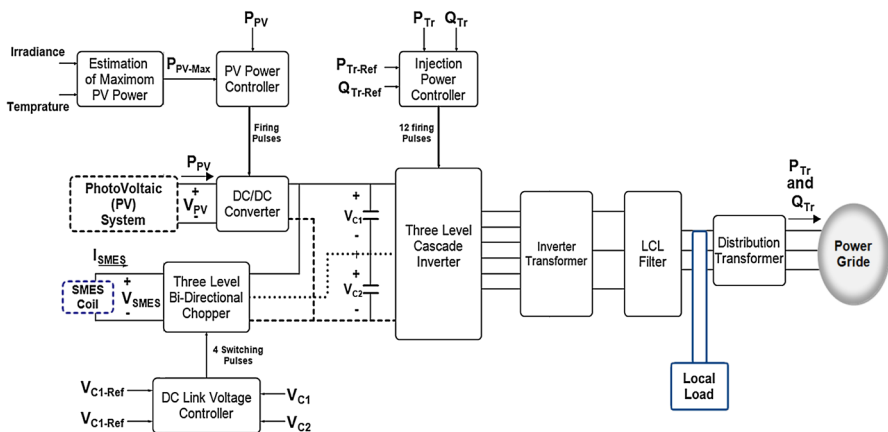


Fig. 1 The introduced structure of distributed generation in this paper based on SMES and photovoltaic

injected active and reactive power into the grid is performed through inverter switching control and the output of the inverter after connecting to a transformer and a filter, is connected to a transformer inside the ground substation of the distribution network.

The control process of the different parts of the system including the DC-link voltage and the output power of photovoltaic system and also active and reactive power flow into the grid and finally, estimating the maximum power of photovoltaic system are performed based on the following steps:

- The maximum power of photovoltaic (PV) system in a particular temperature and radiation is estimated.
- The output power of photovoltaic system is controlled around the maximum value by a DC/DC converter
- DC-link's voltage just is the capacitor bank voltage is regulated by chopper switching control.
- Regulation of active and reactive power flow into the grid is performed by inverter switching control. Two open-loop fuzzy controllers regulate both the phase angle of the wave modulation and its modulation index.

3 Photovoltaic system, the accessible power estimation and receiving

A photovoltaic (PV) system is consisted of a number of series/parallel cells as shown in Fig. 2 which in [7, 8], the way of their modeling is explained. In the modeling process of the mentioned system, a current source which its value depends upon solar radiation is used according to Fig. 2 and the voltage and current equations are as (1)–(4). In Fig. 3a the voltage and current curve of a sample PV array with parameters according to Table 1 is shown and in Fig. 3b the maximum power curves in different temperatures and radiations are shown. Moreover, from the resulted curves, the dependence of the array power on the temperature and radiation could be clearly concluded. As it is clear from Fig. 3b, the maximum power of array in each temperature and radiation takes place for a particular conditions and to use the array optimally, it is required that the maximum power point is tracked and is received from photovoltaic system. The curves from Fig. 3 and the parameters from Table 1 are used in the simulation

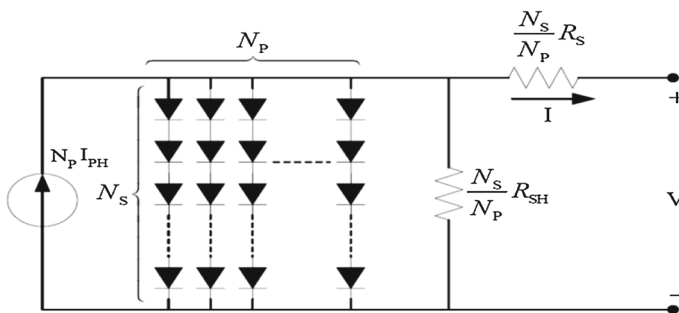


Fig. 2 Photovoltaic system model consisting of series/parallel cells

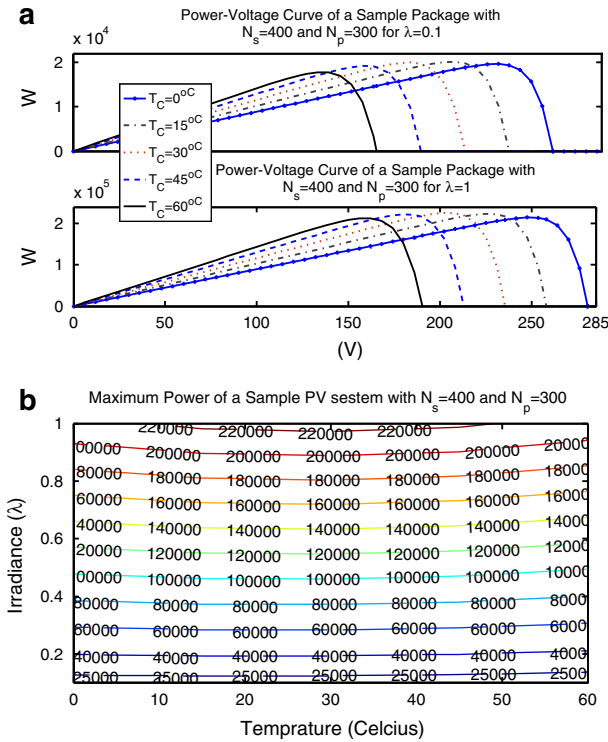


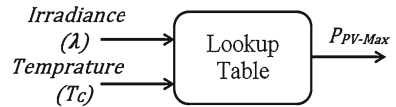
Fig. 3 **a** The power–voltage curve of a sample photovoltaic system to be used in simulation. **b** The maximum power of a sample photovoltaic system based on radiation and temperature to be used in simulation

Table 1 The parameters of a sample photovoltaic package

Description	Symbol	Value	Unit
The number of series cells	N_S	400	–
The number of parallel cells	N_P	300	–
The temperature effect coefficient on the current of cell	K_I	0.03	Ampere/Celsius
The open circuit voltage of the package for reference temperature and radiation	V_{oc}	$400 \times 0.6 = 240$	Volt (V)
The short circuit current of the cell	I_{SC}	$300 \times 3.6 = 1,090$	Ampere (A)
The reference temperature	T_{ref}	27 °C	Celsius
The parallel resistor in cell model	R_{SH}	10	KΩ
The series resistor in cell model	R_S	10	μΩ
The ideal coefficient of the cell	A	3.3	–

part for future sections of paper. Noticing to mention that from the data of Fig. 3b and Table 1, the tracking of the maximum power point is achievable according to Fig. 4.

Fig. 4 Data table to be used for estimating the maximum power of photovoltaic system



$$I_{PH} = [I_{sc} + K_I(T_c - T_{ref})] \cdot \lambda \tag{1}$$

$$I_{RS} = \frac{I_{sc}}{e^{\frac{q \cdot V_{oc}}{N_s \cdot k \cdot A \cdot T_c}} - 1} \tag{2}$$

$$I_S = I_{RS} \left(\frac{T_c}{T_{ref}} \right)^3 \cdot e^{\frac{q \cdot E_G \cdot \left(\frac{1}{T_{ref}} - \frac{1}{T_c} \right)}{k \cdot A}} \tag{3}$$

$$I = N_p \cdot I_{PH} - N_p \cdot I_s \left[e^{\frac{q \left(\frac{V}{N_s} + \frac{R_s \cdot I}{N_p} \right)}{k \cdot T_c \cdot A}} - 1 \right] - \frac{\frac{N_p V}{N_s} + R_s \cdot I}{R_{sh}} \tag{4}$$

With regard to the proposed structure in Fig. 1, it is required that the power is received from the photovoltaic system. For this reason, a DC/DC converter as Fig. 5 is used and for a particular switching frequency, the switching pulse width is determined by a PI-controller. PI-controller determines the constant value to be compared with saw-tooth wave with a particular switching frequency as shown in Fig. 5 and as a result, the power received from photovoltaic system is regulated according to the determined value from data table.

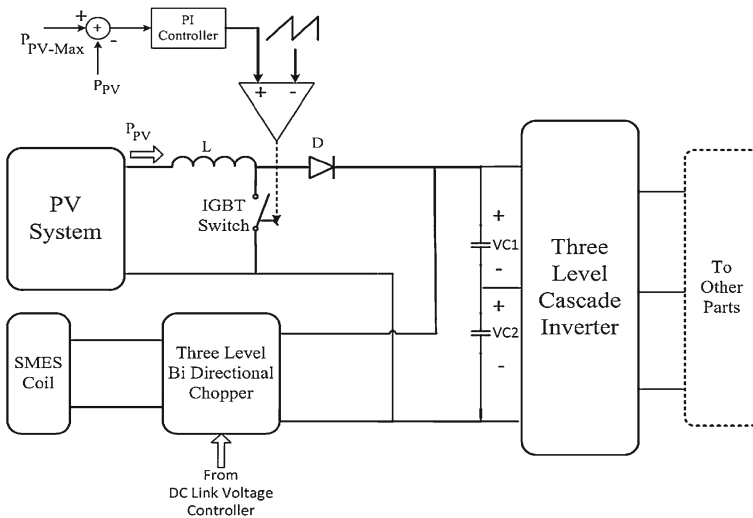


Fig. 5 The way of controlling the extracted power from the photovoltaic system

4 Super conductive magnetic energy storage (SMES), bi-directional-three-level chopper and DC-link voltage control

According to Figs. 1 and 5, SMES and photovoltaic system (PV) together are used as distributed generation resource. In this part, the way by which DC-link voltage is controlled is presented knowing that the DC-link voltage is the common output of bi-directional-three-level chopper and DC/DC converter. The bi-directional-three-level chopper is shown in Fig. 6 and it could be seen from Fig. 6 that the chopper’s input is connected to SMES and its output is connected to the capacitor bank. It is a key note that the SMES coil in which modeled with two lumped components include of an inductance (L_{SMES}) and also a lump resistance (R_{SMES}) is a current feed component which cannot be open circuit anyway. As this moment, a proper converter should be used as an interface between the coil and DC link which is the shown chopper in Fig. 6. Now, a relative switching controller should be designed for coil’s current path in charge, discharge and hold modes. The chopper consists of four switch and 16 switching states which 7 states are used according to Table 2 and the input–output relation is based on the mentioned table. The chopper structure with current path in operating modes, have been illustrated by Fig. 7.

The control operation of the chopper must be in a way that the output voltage of the chopper just is the DC-link voltage of the distributed generation system, is fixed on a

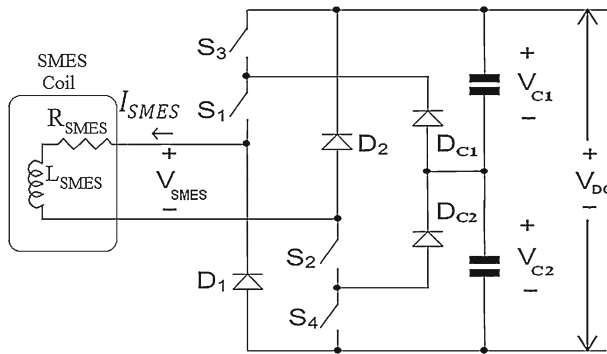


Fig. 6 Bi-directional-three-level chopper

Table 2 The seven modes and operation states of the bi-directional-three-level chopper

Mode number	V_{SMES}	S1 S2 S3 S4	Operation case
1	$V_{c1} + V_{c2}$	1111	Charge
2	V_{c2}	1101	Charge
3	V_{c1}	1110	Charge
4	0	1100	Hold
5	$-V_{c2}$	0100	Discharge
6	$-V_{c1}$	1000	Discharge
7	$-(V_{c1} + V_{c2})$	0000	Discharge

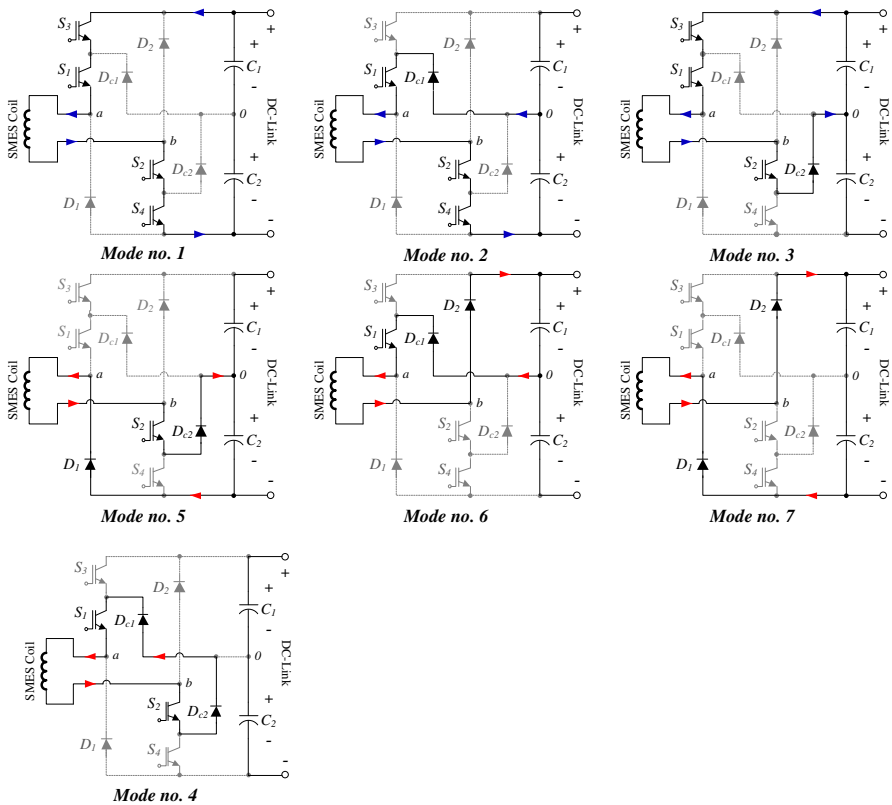


Fig. 7 The chopper structure and current path in operating modes

desirable value and the voltage of the capacitors is equal and half the DC-link voltage according to relations (5, 6).

$$V_{DC} = V_{DC-Ref} \tag{5}$$

$$V_{c1} = V_{c2} = \frac{V_{DC-Ref}}{2} \tag{6}$$

The operation modes of chopper listed in Table 2 are considered, following the change of operation modes, the charging and discharging process between SMES and DC-link capacitors takes place and DC-link voltage would be controlled to achieve the above-mentioned relations. For this reason, the algorithm which is shown as flowchart in Fig. 8 is used which was first proposed by the researcher of this paper. The advantages of this algorithm could be described as its wide area of voltage controllability and quick-responding and desirable dynamic. If f_{ch} is considered as chopper switching frequency, a reference wave is used during the switching process and as the rising edge is detected, the operation mode of the chopper is changed in order to apply the control algorithm. The process is shown in Fig. 8.

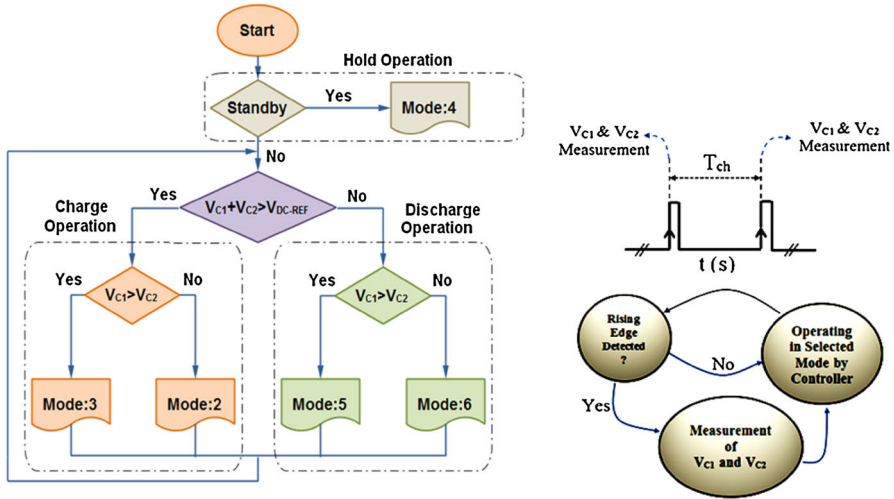


Fig. 8 The flowchart of DC-link voltage control through changing the modes of bi-directional-three-level chopper

5 Three-level inverter and the connected three-phase transformer

After controlling and fixing the DC-link voltage, it is required that this voltage is transformed into 3ph AC voltage. To achieve this goal, in this paper a cascade three-level inverter and the transformer connected to it, is used as in Fig. 9. The switching algorithm of this inverter is based on carrier and modulation waves, in which two triangular waves as carrier waves and three sinusoidal waves with base frequency as modulation waves determine the inverter switching. The switching hardware and also the switching method are described in Fig. 10 for a sample leg. If modulation waves as (7) are considered, the main component of 3ph wave of inverter’s output would be at the same phase and the same frequency as the modulation waves. The more the frequency of the carrier wave becomes; the better would be the harmonic spectrum

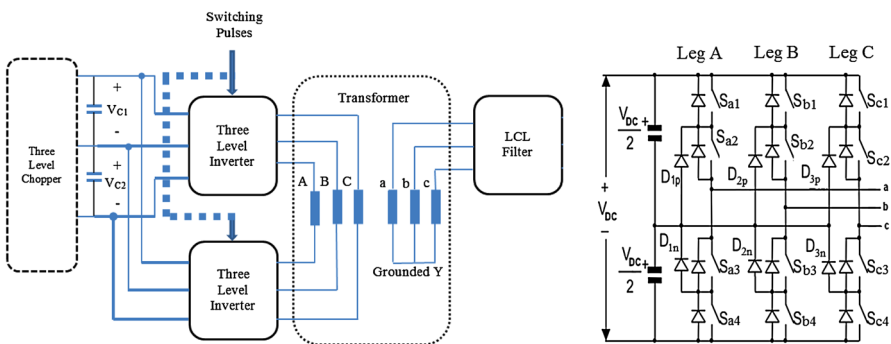


Fig. 9 The structure of three-level inverter used in this paper

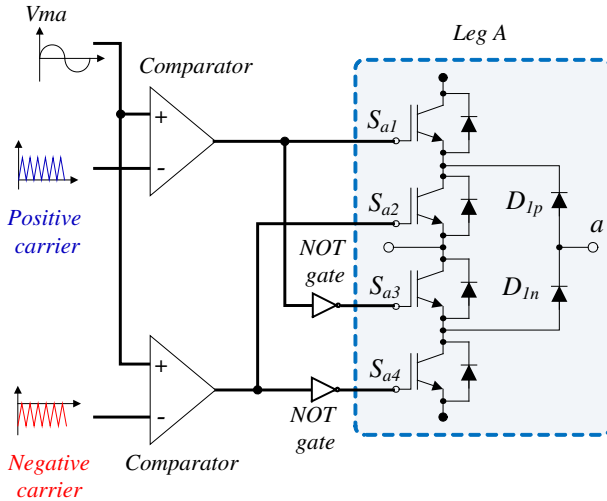


Fig. 10 SPWM switching of inverter for leg A as a sample leg

of the inverter’s output. In reality, comparing the modulation and carrier waves, the trigger pulses of inverter’s switches are determined in a way that the main component of inverter’s output would be at the same phase and the same frequency as the modulation waves. In such conditions, considering the value equals to 1 for the magnitude of the carrier wave, the coefficient $0 < A < 0.85$ is considered for modulation waves. The switching technique of three-level inverter and its control process is described in [22].

$$\begin{aligned}
 V_{ma} &= A \times \sin(2\pi f \cdot t + \varphi) \\
 V_{mb} &= A \times \sin(2\pi f \cdot t + 120 + \varphi) \\
 V_{mc} &= A \times \sin(2\pi f \cdot t - 120 + \varphi)
 \end{aligned}
 \tag{7}$$

6 LCL filter

For filtering the inverter’s output voltage, it is required that a low pass harmonic filter is used and a LCL filter can be a good choice which is shown in Fig. 11. In this filter the transfer function and resonance frequency are approximately independent of the load amount. The existing relations for this filter are written as (8)–(10). Where, f_0 denotes to cut-off frequency of filter.

$$\frac{V_O(S)}{V_i(s)} = \frac{R}{L_1 \cdot L_2 \cdot C \cdot S^3 + L_1 \cdot R \cdot C \cdot S^2 + (L_1 + L_2)S + R}
 \tag{8}$$

$$f_0 = \frac{1}{2\pi} \times \sqrt{\frac{L_1 + L_2}{L_1 \cdot L_2 \cdot C}}
 \tag{9}$$

Fig. 11 The single line diagram of LCL filter connected to the inverter's output

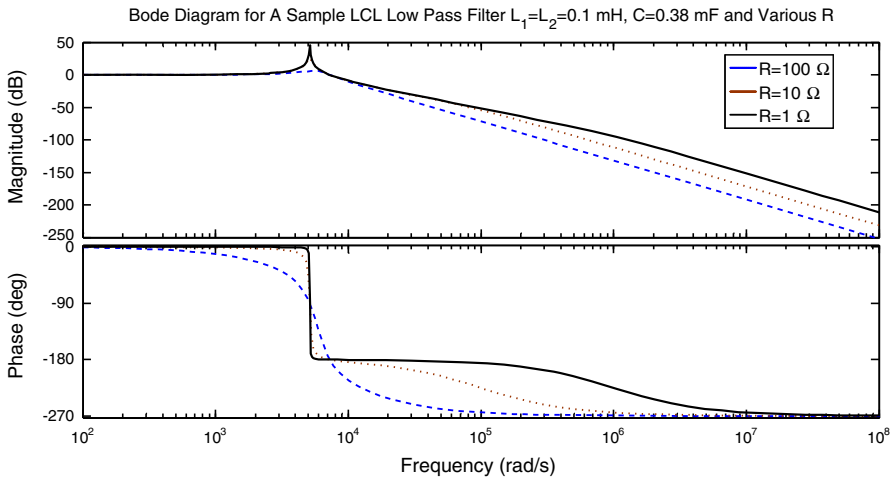
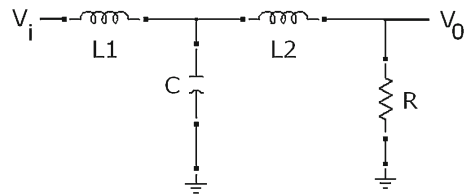


Fig. 12 Bode diagram of the LCL filter for sample values

$$f_0 = \frac{1}{2\pi} \times \sqrt{\frac{3}{2L_2 \cdot C}} \tag{10}$$

Considering f_0 and f as the cut-off and base frequencies, in order to have $f_0 = k \cdot f$, the capacitor value is calculated according to (11). Bode diagram of this filter for $k = 20$, $f = 50$ Hz for several amounts of load is as Fig. 12 and it could be clearly seen that the transfer function is virtually independent of the load amount.

$$C = \frac{3}{8\pi^2 \cdot k^2 \cdot f^2 \cdot L_2} \tag{11}$$

The output power from photovoltaic system and the also active and reactive power fellow into the grid must be controllable. To achieve the mentioned goal, two closed-loop fuzzy controllers are used regarding that in controllers, phase angle and the magnitude of modulation waves are regulated and the designed algorithm is shown in Fig. 13. In Table 3 the inputs and outputs of fuzzy controllers are listed. The constants K_e , K_d , K_o are regulated to reach the better operation of controllers.

For designing the phase controller, the membership functions and fuzzy rules are designed according to Figs. 14, 15 and Table 4 in which the signs nvb, nb, nm, ns, z, ps, pm, pb, pvb are described as ‘negative very big’, ‘negative big’, ‘negative medium’, ‘negative small’, ‘zero’, ‘positive small’, ‘positive medium’, ‘positive big’ and ‘posi-

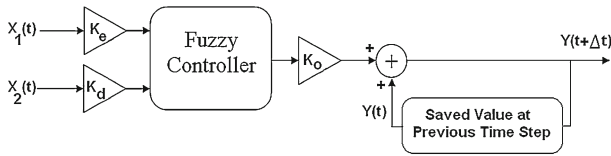


Fig. 13 The structure of two fuzzy controllers for controlling the transmitted active and reactive power into the grid

Table 3 The inputs and outputs of closed-loop fuzzy controller for controlling the transmitted active and reactive power

	$X_1(t)$ (error)	$X_2(t)$ (error rate)	$Y(t)$ (output)
P controller	$\Delta P(t) = P_{Tr-Ref}(t) - P(t)$	$\Delta P(t) - \Delta P(t - \Delta t)$	$\varphi(t)$
Q controller	$\Delta Q(t) = Q_{Tr-Ref}(t) - Q(t)$	$\Delta Q(t) - \Delta Q(t - \Delta t)$	A

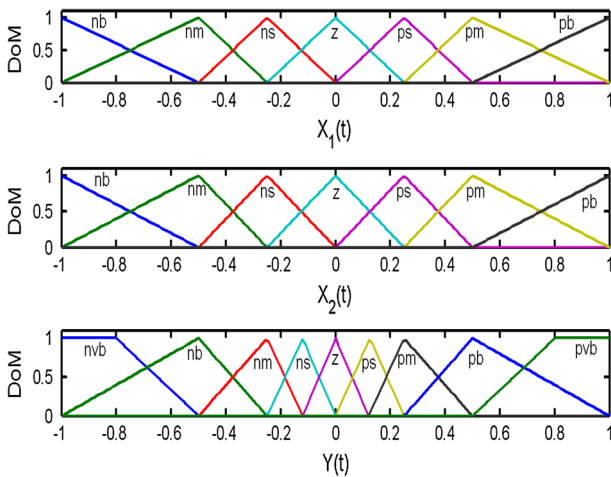


Fig. 14 The membership functions of fuzzy controllers

tive very big’ in order. In Figs. 12 and 13, vectors are normalized and are between 0 and 1.

In Fig. 16 the general block diagram of the system is shown. Inputs and outputs are shown in different subsystems. With regard to this structure, chopper controller controls the capacitors DC-link voltage and two controllers control the injected active and reactive power into the grid. These two controllers are the fuzzy controllers described in the previous part and it should be known that the controlling process takes place by regulating the modulation waves. Chopper controller regulates DC-link voltage by changing the operation mode in every period of the switching period.

Fig. 15 The fuzzy surface of fuzzy controllers

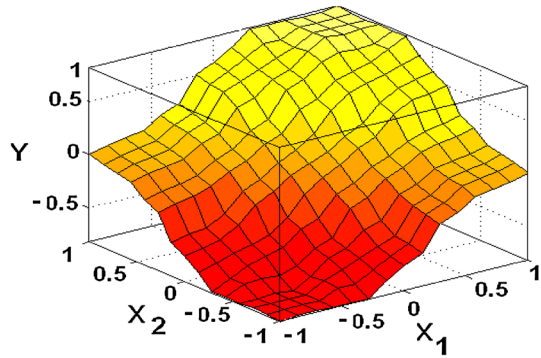


Table 4 The applied fuzzy rules to the fuzzy controllers of transmitted active and reactive power into the grid

Fuzzy rule base		X_1						
		nb	nm	ns	z	ps	pm	pb
X_2	nb	nvb	nvb	nvb	nb	nm	ns	Z
	nm	nvb	nvb	nb	nm	ns	z	ps
	ns	nvb	nb	nm	ns	z	ps	pm
	z	nb	nm	ns	z	ps	pm	pb
	ps	nm	ns	z	ps	pm	pb	pvb
	pm	ns	z	ps	pm	pb	pvb	pvb
	pb	z	ps	pm	pb	pvb	pvb	pvb

7 Simulation

In order to simulate the structure proposed in Fig. 1 and to demonstrate the efficiency of control algorithm in different subsystems, several simulations are performed in MATLAB Environment. The system parameters are according to Table 5 and the parameters pertaining to photovoltaic system are according to Table 1 and Figs. 3 and 4.

With regard to system parameters, for initial current of $I_0 = 1,000$ A in magnetic energy storage element, the SMES capacity is equal to $W_{SMES} = \frac{1}{2} \cdot L \cdot I^2 = 1 MJ$ and the maximum power of photovoltaic system for maximum radiation according to Figs. 3 and 4 is roughly equal to 200 KW. The considered local load is equal to 80 KW. It is known that the received power from photovoltaic system by data table for each temperature and radiation is regulated on the maximum value and as a result if the transmitted power into the grid is more than the power of photovoltaic system, the remainder of power is produced by SMES and the element is discharged. On the other hands, if the transmitted power into the grid is less than the power of photovoltaic system, the element is charged and its current rises. Now the assumption is that the initial current of energy storage inductance is equal to 1,000 A and the temperature is at 30 °C and the radiation is reached from 100 to 50 % at $t = 5$ s (even though

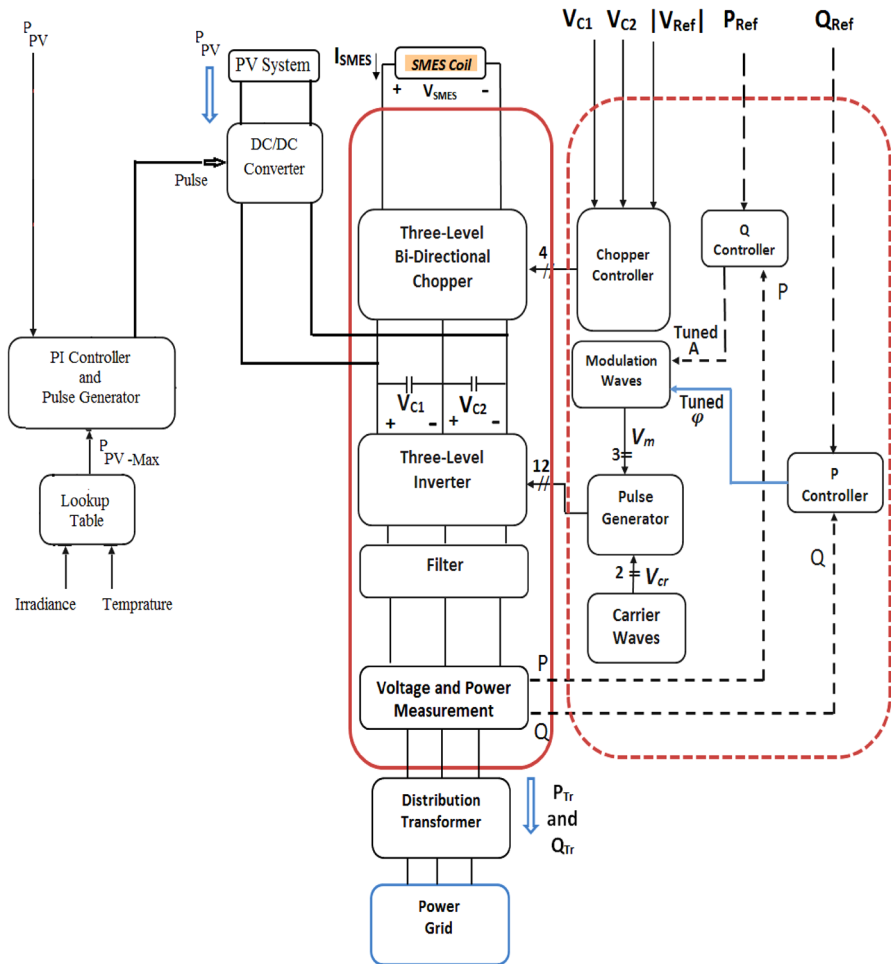


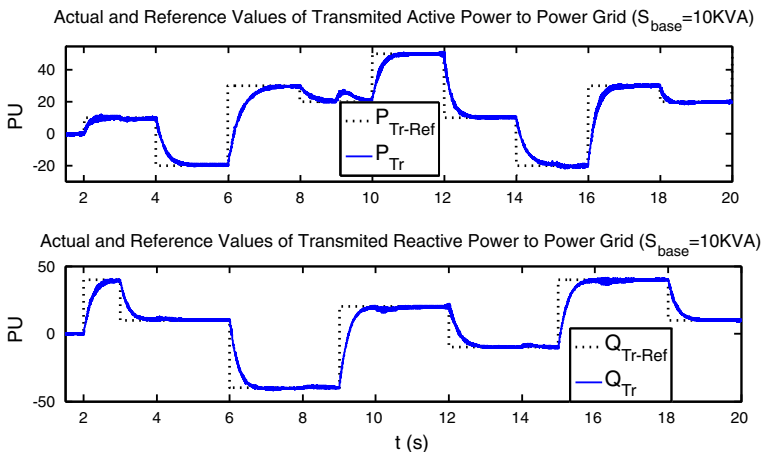
Fig. 16 The control structure block diagram

such change is unlikely in real world). In order to test the fuzzy controllers operation, some changes for transmitted active and reactive power into the grid is considered according to Fig. 17 and simulation results are shown in Figs. 17, 18, 19, 20 and 21 and the results are described.

In Fig. 17, the reference active and reactive power is changed in each 2 s. As it is clear from the figure, the fuzzy controllers, based on the reference values, follow the transmitted power acceptably. The regulation from fuzzy controllers is performed through regulating both the phase angle and the magnitude of the inverter's modulation waves as it is shown in Fig. 18. In Fig. 19, in order to demonstrate the operation of the chopper's controller, the voltage across the energy storage inductance and also the operation modes of the chopper are shown. As it is clear from the figures, the controller performs the DC-link voltage control by changing the operation mode of the chopper for each switching period of the chopper. In Fig. 20, the operation of power

Table 5 The system parameters for simulation

Symbol	Definition	Value	Unit
L_{SMES}	The value of the inductance in the magnetic energy storage element	2	H
R_{SMES}	The value of the internal resistor in the magnetic energy storage element	2	$\mu\Omega$
C_1, C_2	DC-link capacitors	0.8	f
V_{DC-Ref}	DC-link reference voltage	820	v
$L_{DC/DC}$	The inductance used in the DC/DC converter	100	mH
L_1, L_2	The inductances available in the LCL filter	100	μ H
C	The capacitor available in the LCL filter	380	μ f
R_{on-sw}	The resistor of switches used in the converters in connected position	100	$\mu\Omega$
f	The base system frequency	50	Hz
S_{rate}	The rated power of the transformer connected to the grid and the inverter	1	MVA
$f_{sw-DC/DC}$	The switching frequency of the chopper connected to the photovoltaic system	2.5	KHz
$f_{sw-Chopper}$	The switching frequency of the chopper connected to the energy storage element	30	KHz
R_t	The resistance of the transformer windings	0.0002	Pu
L_t	The inductive quality of the transformer windings	0.08	Pu
N_1/N_2	The transform ratio of the transformers connected to the grid	0.4/20	Kv
N_1/N_2	The transform ratio of each phase of the transformer connected to the inverter	425/133	v

**Fig. 17** The way of regulating the transmitted active and reactive power into the grid by fuzzy controllers

controller in photovoltaic system is shown, in which the output of the PI-controller is connected to DC/DC converter and also the power regulation of photovoltaic system on its maximum value is shown. In Fig. 21, as the radiation of the environment is

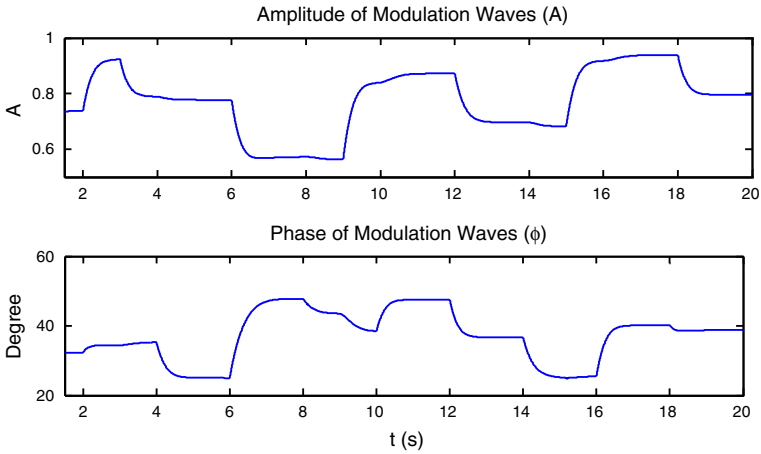


Fig. 18 The way of regulating the magnitude and phase of the inverter’s modulation waves for regulating the active and reactive power

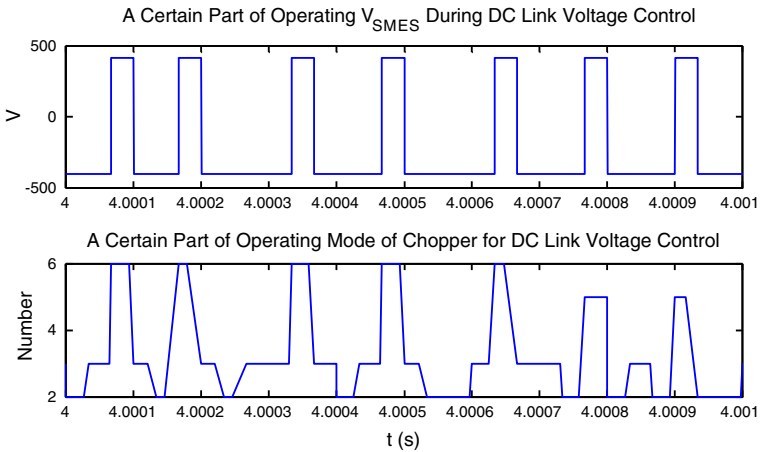


Fig. 19 The operation modes of chopper for controlling the DC-link voltage and the voltage across the magnetic energy storage inductance

changed, the maximum power of photovoltaic system is changed consequently and as a result, the controller changes the converter switching by changing the output of the PI-controller in a way that the output power from the photovoltaic system is regulated on its reference value acceptably. In middle part of Fig. 21, the simulation results for the current of the SMES, DC-link voltage and the flowed active power into the grid are shown. As it is understood from the middle part of the Fig. 21, whenever the received power from the photovoltaic system exceeds the addition of the local load power and the transmitted power into the grid, the remainder of power flows into the storage element (SMES) through the chopper and the current of the storage element rise which mean the SMES charging. Such condition could be clearly seen during the time from 4 to 6 s. On the opposite side, if the received power from the photovoltaic

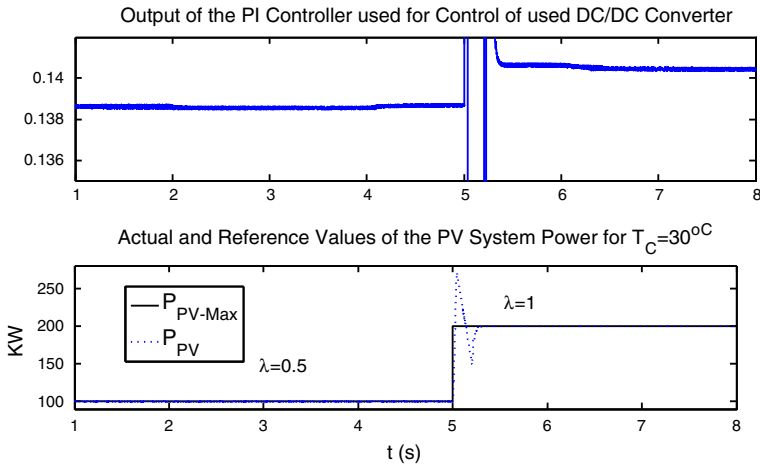


Fig. 20 The power of photovoltaic system and the modulation waves of the DC/DC converter for regulating the power of photovoltaic system for 1–8 s

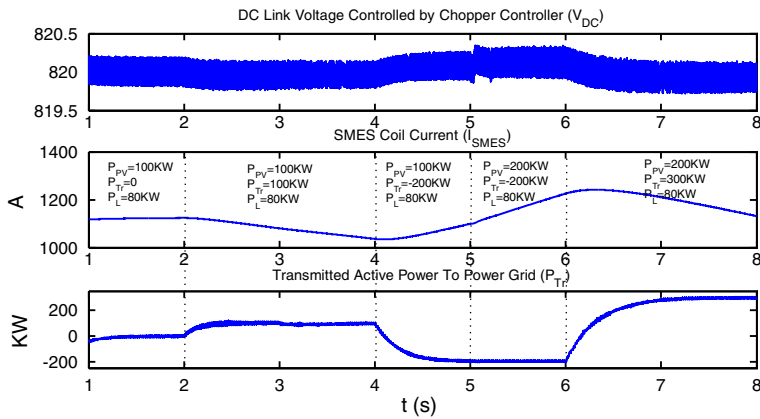


Fig. 21 The DC-link voltage, current of the SMES coil and flowed power to power grid for 1–8 s

system falls below the addition of the local load power and the transmitted power into the grid, the remainder of power is produced by the storage element and this process will result in the current fall. Such condition usually takes place after 6 s.

8 Conclusion

In this paper a novel structure for distributed generation system based on the SMES and photovoltaic system together with necessary controllers were introduced. Two fuzzy controllers were used to regulate the transmitted active and reactive power into the grid on the desirable reference value and a PI-controller was used to regulate the extracted power from the photovoltaic system on the maximum value which is determined according to a data table consisting of radiation and temperature. The

control of the DC-link voltage was performed by the chopper which is connected to the superconductor and a new control algorithm for the mentioned chopper was presented. The simulation results have verified the efficiency and capabilities of designed control algorithms and introduced structure and led to the accurate operation. The advantages of this paper over the others are as follows:

- Proposing a new algorithm for controlling the three-level chopper which is connected to the superconductor
- The accurate and thorough control of the DC-link voltage with fast dynamic
- The direct connection of superconductor to the chopper without using a filter
- The composition of superconductor and photovoltaic system as distributed generation resource
- Having a comprehensive control over system voltage and power.

Some of the above-mentioned advantages are first proposed in this paper. For further research, some ideas such as ‘proposing and comparing the operation of other controllers with active and reactive power fuzzy controllers’ and ‘the more accurate modeling of superconductive elements with non-compressed element’ and ‘targeted regulation of the transmitted active and reactive power into the grid based on the peak hours and local load values’ and also ‘the way of distributed generation system is landing introduced in this paper’ are proposed.

References

1. Mathiesen, B.V., Lunda, H., Karlsson, K.: 100 % Renewable energy systems, climate mitigation and economic growth. *Appl. Energy* **88**(2), 488–501 (2011)
2. Genoese, F., Genoese, M.: Assessing the value of storage in a future energy system with a high share of renewable electricity generation. *J. Energy Syst.* **5**(1), 19–44 (2014)
3. Molina, M.G.: Distributed energy storage systems for applications in future smart grids. In: Latin America Conference and Exposition on Transmission and Distribution (2012)
4. Ali, M.H., Wu, B., Dougal, R.A.: An overview of SMES applications in power and energy systems. *IEEE Trans. Sustain. Energy* **1**(1), 38–47 (2010)
5. Molina, M.G., Mercado, P.E., Watanabe, E.H.: Improved superconducting magnetic energy storage (SMES) controller for high-power utility applications. *IEEE Trans. Energy Convers.* **26**(2), 444–456 (2011)
6. Nielsen, K.E., Molinas, M.: Superconducting magnetic energy storage (SMES) in power systems with renewable energy sources. In: IEEE International Symposium on Industrial Electronics (ISIE) (2010)
7. Naderi, P., Alizadehp, M.R., Azizianfard, M.: A novel controlling method for the superconducting magnetic energy storage system as a distributed generation source; full modelling, design and simulation. *Int. J. Sustain. Energy* **33**(3) (2013)
8. Amin, M.M., Moussa, H.B., Mohammed, O.A.: Wide area measurement system for smart grid applications involving hybrid energy sources. *J. Energy Syst.* **3**(1), 3–21 (2012)
9. Tsai, H.-L., Tu, C.-S., Su, Y.-J.: Development of generalized photovoltaic model using MATLAB/SIMULINK. In: Proceedings of the World Congress on Engineering and Computer Science, San Francisco (2008)
10. Naderi, P.: Distributed generation using battery/photovoltaic system: modeling and simulation with relative controller design. *J. Solar Eng. Sci.* **135**(2) (2013)
11. Carmeli, M.S., Dezza, F.C., Mauri, M., Marchegini, G.: Control strategies and configurations of hybrid distributed generation systems. *J. Renew. Energy* **41**, 294–305 (2012)
12. Bruni, G., Cordiner, S., Galeotti, M., Mulone, V., Nobile, M., Rocco, V.: Control strategy influence on the efficiency of a hybrid photovoltaic-battery-fuel cell system distributed generation system for domestic applications. In: 68th Conference of the Italian Thermal Machines Engineering Association, vol. 45, pp. 237–246 (2014)

13. Fadil, E., Giri, H., Yahya, F., Erguig, A.: Nonlinear control of hybrid photovoltaic/fuel cell distributed generation system. In: 11th IFAC International Workshop on Adaptation and Learning in Control and Signal Processing, pp. 665–670 (2013)
14. Pearco, J.M.: Expanding photovoltaic penetration with residential distributed generation from hybrid solar photovoltaic and combined heat and power systems. *J. Energy* **34**(11), 1947–1954 (2009)
15. Wang, C.: Modeling and control of hybrid wind/photovoltaic/fuel cell distributed generation systems. Ph. D. Thesis, Montana State University (2006)
16. Alizadeh, M.R., Mohammadpour, H.A.: An optimized SVPWM switching strategy for three-level NPC VSI and a novel switching strategy for three-level two-quadrant chopper to stabilize the voltage of capacitors. *J. Energy* **35**(12), 4917–4931 (2010)
17. Shukla, A., Ghosh, A., Joshi, A.: Control of DC capacitor voltages in diode-clamped multilevel inverter using bidirectional buck-boost choppers. *IET Power Electron.* **5**(9) (2012)
18. Peng, D., Lee, D.H., Lee, F.C., Borojevic, D.: Modulation and control strategies of ZCT three-level choppers for SMES application. In: 31st Annual Power Electronics Specialists Conference, pp. 121–126 (2000)
19. Monge, S.B., Alepuz, S., Bordon, J.: A novel bidirectional multilevel boost-buck DC–DC converter. In: Energy Conversion Congress and Exposition, pp. 707–714 (2009)
20. Frank, S., Steponavice, I., Rebennack, S.: Optimal power flow: a bibliographic survey I formulations and deterministic methods. *J. Energy Syst.* **3**(3), 221–258 (2012)
21. Frank, S., Steponavice, I., Rebennack, S.: Optimal power flow: a bibliographic survey II Non-deterministic and hybrid methods. *Journal of Energy Systems* **3**(3), 259–289 (2012)
22. Bose, B.K.: Modern Power Electronics and AC Drives. Prentice-Hall, New Jersey (2002)